International Journal of Rock Mechanics & Mining Sciences 138 (2021) 104644

Contents lists available at ScienceDirect

International Journal of Rock Mechanics and Mining Sciences

journal homepage: http://www.elsevier.com/locate/ijrmms

Discrete fracture matrix modelling of fully-coupled CO_2 flow – Deformation processes in fractured coal

K.H.S.M. Sampath [a], M.S.A. Perera [a,*], D. Elsworth [b], S.K. Matthai [a], P.G. Ranjith [c], Li Dong-yin [d]

[a] Department of Infrastructure Engineering, The University of Melbourne, Engineering Block B, Grattan Street, Parkville, Victoria, 3010, Australia
[b] Energy and Mineral Engineering, G3 Center and EMS Energy Institute, Pennsylvania State University, University Park, PA, 16802, USA
[c] Department of Civil Engineering, Monash University, Clayton Campus, Victoria, 3800, Australia
[d] School of Energy Science and Engineering, Henan Polytechnic University, Jiaozuo, 454000 12, China

ARTICLE INFO

Keywords:
Coal
CO2 interaction
Hydro-mechanical coupling
Sorption-swelling
DFM modelling

ABSTRACT

CO_2 interaction causes complex mechanical deformations and flow modifications in coal, depending on the spatial disposition of the fracture-matrix system. Sorption-induced matrix swelling reduces the local fracture aperture and correspondingly the fracture permeability, consequently influencing gas flow throughout the seam. Since these modifications are highly -heterogeneous and -localized, an explicitly-represented geometric model is essential for the accurate modelling of the fully-coupled process. In this study, the CO_2 flow – coal deformation process is implemented in a numerical model at the scale of coal constituents (i.e. matrix blocks and cleats), through the inclusion of a spatially distributed 3D – discrete fracture matrix (DFM) network. Fracture geometry is generated from a stochastically simplified 2D fracture network obtained from micro-CT imaging. The approach is initially validated against experimental results from a single-fractured coal specimen and the analysis extended to the complex fracture geometry. The spatial and temporal evolutions of fracture/matrix pressure, adsorbed mass of CO_2, adsorption-induced swelling, alterations in local fracture aperture and permeability, and contact modelling at fully fracture closure are specifically analysed with comparison against no-swelling behaviour. Results indicate that the high-permeability fracture pathways provide initial easy access for the CO_2 to diffuse into the coal matrix, causing sorption-induced matrix swelling. Although the individual matrix blocks exhibit a slight shrinkage immediately upon injection of high fluid pressures within the fractures, sorption-induced swelling rapidly overcomes this, resulting in an overall volume expansion at full pressure equilibration. This is turn causes a significant reduction in fracture aperture and permeability. The magnitude of the local fracture aperture reduction depends on the swelling behaviour of the bounding matrix, that leads to essentially full-closure of small fractures, causing significant localized flow modifications to further CO_2 injection in the vicinity of the particular fractures. The contact modelling approach identifies the timing and locations of fully-closing fractures in the complex geometry, where butt cleats exhibiting initial small apertures are prone to fully-close, compared to larger aperture face cleats that retain flow.

1. Introduction

High growth in population coupled with rapid industrialization have increased annual rate of global primary energy consumption by 2.9%, comprising the fastest growth rate since 2010. Consequently, global CO_2 emissions from fossil fuel combustion was elevated by 1–1.5% in 2019, with concomitant impacts on environment and health.[1,2] Numerous measures address this issue, specifically focusing on minimising levels of atmospheric CO_2 and impacts on global temperatures. Among a number of viable options, CO_2 geo-sequestration in deep coal seams has been identified as a promising solution - coal serves as a sorptive reservoir for the CO_2 with significant worldwide capacity, longevity and security. Besides, the greater adsorption potential of CO_2 to coal, relative to methane, allows CO_2 flooding to concomitantly boost the sweep efficiency of native methane, enhancing coalbed methane (CBM) production and further offsetting the cost of CO_2 storage. This, in turn increases the contribution of natural gas to total energy consumption, with a significant increment of 4.7% apparent in 2019, representing one of the

* Corresponding author. Department of Infrastructure Engineering, The University of Melbourne, Room: B 209, Engineering Block B Building 175, Grattan Street, Parkville, Victoria, 3010, Australia.
E-mail address: samintha.perera@unimelb.edu.au (M.S.A. Perera).

https://doi.org/10.1016/j.ijrmms.2021.104644
Received 8 April 2020; Received in revised form 2 September 2020; Accepted 4 January 2021
Available online 16 January 2021

strongest growth-rates in utilization in over 30 years.[1,2]

Coal is an extremely complex and heterogeneous material. This is due to its unique process of formation – coalification, and in particular due to the complex geometry of the resulting natural cleat system.[3] Injection of large quantities of CO_2 into coal reservoirs triggers complex coal-CO_2 interactions, triggering a complex hydro-mechanical response, in particular, that due to adsorption-induced swelling. The combined roles of the fracture network, ambient stress and gas pressure contribute to the fully-coupled response to gas transport, adsorption and the consequent swelling, that make the analysis rather complex.[4,5] For instance, the permeability, that generally governs gas transport within the coal reservoir is mediated by cleat aperture.[6] Thus, any change in cleat aperture, driven either by effective stresses or sorption-induced swelling, will modify the coal permeability and ultimately impact gas transport throughout the seam.[7]

Changes in the gas flow behaviour and the subsequent reduction in CO_2 injectivity due to swelling-induced permeability alteration are investigated by previous studies – by conducting experiments at both laboratory- and field-scales and by developing numerical and analytical models representing specific reservoir conditions.[8–12] For instance, a substantial drop in CO_2 injectivity into the seam was observed in the Fruitland Coal Fairway CO_2 sequestration project, with a reported drop from an initial 7.08×10^4 m^3/day to 1.42×10^4 m^3/day after about one year.[9] This observed reduction in CO_2 injectivity substantially hinders the efficiency of sequestration projects. Laboratory-scale tri-axial experiments replicating *in-situ* stress conditions also reveal large permeability reductions with increasing injection pressures, especially beyond the critical point of CO_2 (i.e. 31.1 °C and 7.38 MPa).[8,10] Based on theoretical and empirical approaches, several permeability evolution models (e.g. Robertson-Christiansen,[13] Palmer-Mansoori,[14] Seidle-Huitt,[15] Cui-Bustin[16] and Shi-Durucan[17]) have been developed to account for the dynamic evolution of coal permeability. However, these models are either single- or multi-continuum models or analytical formulations, which are derived from a scalar porosity variable. Thus, these often fail to address the spatial and temporal variation of fracture permeability in a typical coal reservoir with a complex fracture network. Recognizing the dominant impact of the fracture network on CO_2 flow in fractured coals has prompted the development of discrete fracture matrix (DFM) models, in which fractures are explicitly and discretely represented in the geometric model. Initial approaches assumed the matrix to be impermeable and that fluid flow was restricted to the fracture network.[18] Later DFM models accommodated flow in the matrix to investigate the effect of free and adsorbed gas on gas production in fractured reservoirs including cleat-scale models.[19] For instance, Bertrand et al.[20] recently developed a cleat-scale DFM model to simulate the evolution of coal permeability due to adsorption-induced strain.

In this study, the fully-coupled process of CO_2 flow – coal deformation is implemented in a numerical model at the scale of coal constituents (i.e. matrix blocks and cleats). The spatial and temporal variation of fracture permeability is specifically analysed by including a spatially distributed 3D – discrete fracture matrix (DFM) network, stochastically generated from a reference micro-CT image. Since the fracture network is explicitly represented in the geometric model, the fracture permeability is directly determined as a function of local fracture aperture – defining the local evolution of permeability. A model containing a single fracture is initially developed and validated against experimental observations of permeability evolution to confirm the reliability of the model. The simulation is then extended to DFMs of realistic complexity and large spatial extent. Finally, a comparison between the effect of swelling and no-swelling behaviour on CO_2 flow is presented to highlight the significance of CO_2 adsorption-induced swelling on the modification of flow in coal.

2. Discrete fracture matrix (DFM) modelling approach

Since single- or multi-continuum models provide no geometric distinction between fracture and matrix domains, they fail to evaluate spatial or localized alterations of influential parameters in a complex fracture geometry. In contrast, the DFM modelling approach treats fractures, matrix and interfaces as separate geometric objects. This is essential in modelling complex coal reservoirs, since each feature should be explicitly represented due to their dominating impact on the fully-coupled process.[21] Although DFM modelling is conceptually simpler than continuum modelling, as it avoids the application of transfer functions by explicitly meshing each domain, special care should be taken when defining the geometry to reduce the excessive computational cost. In the context of DFM modelling, unlike mixed-dimensional or hybrid approaches, equidimensional representation of fractures necessitates a very fine mesh to avoid large aspect ratios of the individual cells. Since the current study incorporates the interaction of multiple physical fields, including stress- and time-dependent aperture variation, hydro-mechanical coupling and contact modelling, that interact through both contact interfaces of the fracture surface, an equidimensional DFM modelling approach is appropriate, irrespective of the significant computational burden. Hence, in the current study, we adopt an equidimensional DFM modelling approach, in which the complete problem is decomposed into a set of three problems – one for each sub-domain, linked through a transmission conditions.[22] Further, the local fracture aperture is calculated directly from the deformed geometry, as the distance between the two bounding surfaces of the fracture, and combined with the hydro-mechanical model to simulate the fully-coupled process.

3. Theoretical approach for the hydro-mechanical model

A typical coal structure consists of an orthogonal cleat system, including face cleats and butt cleats, with the coal matrix resident-between *(see* Fig. 1 *(a))*. The cleat network governs the coal permeability, while the intact coal matrix blocks control the diffusion and adsorption of CO_2, and act as the potential reservoir for gas storage.[23,24] In our theoretical approach, the coal structure is conceptualized as a bundle of matchsticks representing individual coal matrix blocks, in which the void spaces between adjacent matrix boundaries form the fracture network *(see* Fig. 1 *(b))*.[25] The fully-coupled process includes CO_2 flow through the fractures, diffusion through the coal matrix, adsorption to potential adsorption sites and the accommodation of adsorption-induced matrix swelling that alters fracture aperture and effective stress and subsequently changes fracture permeability. Implementing this process in a complex DFM model requires a number of theoretical considerations together with defined –stress and –displacement conditions for fracture and matrix domains at relevant boundaries.

In summary, the fully-coupled process adopted in the current study can be segregated as follows: 1) CO_2 flow through the fractures conforms to Darcy's law and CO_2 diffusion through the coal matrix is represented by Fick's second law with stress-invariant diffusion coefficient, 2) CO_2 adsorption and matrix swelling are defined by a Langmuir-type model, 3) coal deformation is coupled to the flow equations through effective stresses and adsorption-induced swelling, 4) fracture permeability is defined as a function of fracture aperture and is calculated locally from the deformed geometry in each solution step, 5) effects of fracture fluid pressure and fracture stiffness are included at fracture-matrix interface boundaries, 6) contact models and frictional interfaces are defined, where the two fracture surfaces contact and 7) stress and displacement boundary conditions are applied to represent *in-situ* reservoir conditions. The following sub-sections describe the complete hydro-mechanical approach in detail, in which the derivations are based on the assumptions that: 1) the coal matrix is an elastic, homogeneous and isotopic continuum, 2) the gas contained within the fractures and pores is ideal, and 3) the system is isothermal.

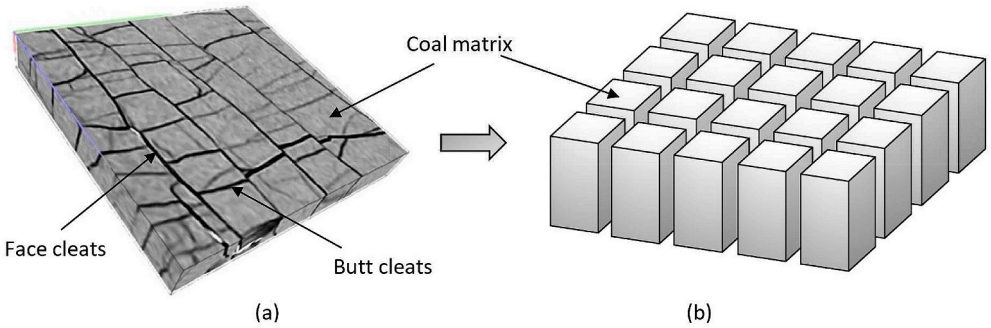

Fig. 1. a) 3D-reconstructed coal segment from Micro-CT imaging, indicating the orthogonal fracture network and the coal matrix blocks,[26] and b) the conceptual reservoir model represented as a bundle of matchsticks separated by fractures.

3.1. Gas-transport system

Gas transport in coal consists of: 1) longitudinal free gas flow in the fracture domain (Ω_f) – that occurs along the fractures, 2) diffusion through the matrix domain (Ω_m) – that accounts for the free and adsorbed gas and 3) transverse flow across the domain interfaces (Γ_{m,f_1} and Γ_{m,f_2}) – that represents gas transfer between fracture and the matrix at fracture-matrix interface boundaries *(see Fig. 2 (a))*.

3.1.1. Gas flow in fractures

The governing equation for gas transport in the fractures is expressed as;

$$\frac{\partial(\varphi_f \rho_{g,f})}{\partial t} + \nabla(\rho_{g,f} q_L) = Q_s \quad [1]$$

where, φ_f is the fracture porosity, $\rho_{g,f}$ is the density of gas in fractures, q_L is the longitudinal flow along the fracture and Q_s is the source/sink term.

As specified by the equation of state (EOS), the density of gas in the fractures is proportional to the gas pressure and is defined as,

$$\rho_{g,f} = \frac{M_g}{RT} p_f \quad [2]$$

where, M_g is the molar mass of gas, R is the universal gas constant, T is the temperature and p_f is the gas pressure in the fracture domain.

The longitudinal gas flow along the fractures is defined by Darcy's law as,[27]

$$q_L = -\frac{k_f}{\mu} \nabla p_f \quad [3]$$

where, k_f is the fracture permeability and μ is the dynamic viscosity of the gas.

Under the assumption that a particular fracture can be defined as conducting flow between two closely-spaced parallel plates formed by adjacent matrix walls and neglecting the fracture roughness, the fracture permeability can be defined as a function of fracture aperture as[28];

$$k_f = \frac{b^2}{12} \quad [4]$$

where, b is the fracture aperture.

In the governing equation for gas transport within fractures, the permeability is a function of the local fracture aperture that varies with the effective stress and the adsorption-induced swelling deformation of the bounding coal matrix. Hence, the fracture flow is coupled to the mechanical deformation.

3.1.2. Gas flow in the matrix

Gas flow within the matrix is established from mass conservation with Fick's second law defining the rate of transport. Assuming that the temporal derivative of the gas content is equal to the spatial gradient of the mass flux,[29] then,

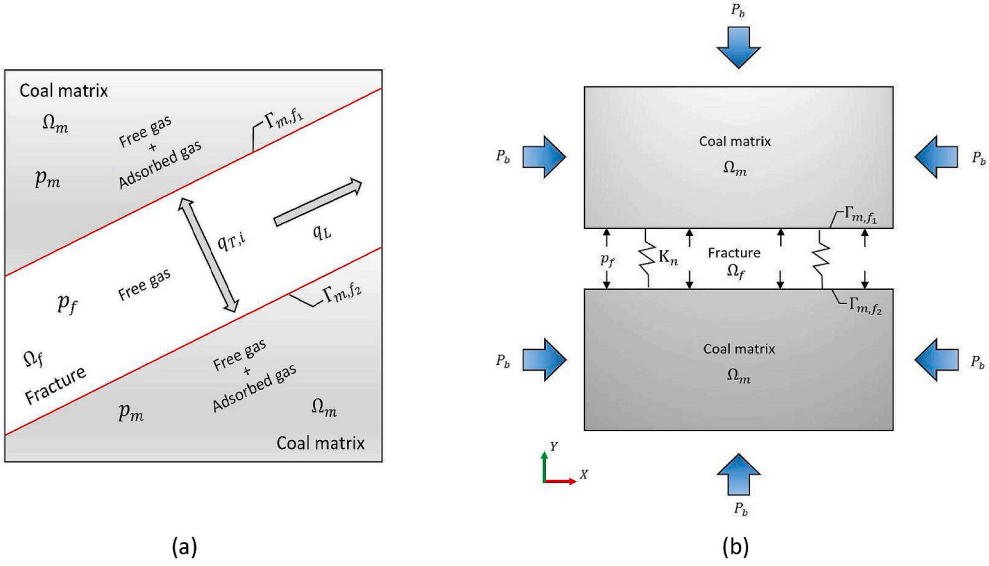

Fig. 2. a) The flow model within the fracture and matrix domains, indicating both longitudinal and transverse flows and the corresponding pressure terms, and b) Definition of the mechanical system of the fractured medium as analogous to a linear spring-closure system.

$$\frac{\partial m}{\partial t} + \nabla . J = 0 \quad [5]$$

where, m is the total gas content and J is the total mass flux.

The total gas content consists of a free-phase gas and an adsorbed-phase gas – that can be expressed in terms of a Langmuir-type model, regardless of the heterogeneity of the adsorption sites in the coal.[30] Thus, the total gas content is expressed as,

$$m = \frac{M_g}{RT}\varphi_m p_m + (1-\varphi_m)\frac{M_g P_a}{RT}\rho_c \frac{V_L p_m}{p_m + P_L} \quad [6]$$

where, φ_m is the matrix porosity, p_m is the matrix pore pressure, P_a is the atmospheric pressure, ρ_c is the density of coal, and V_L and P_L are the Langmuir sorption constant and Langmuir pressure constant, respectively.

Since the combination of coupled processes and the equidimensional modelling approach are both highly complex, we adopt a stress-invariant constant diffusion coefficient to represent gas diffusion in the coal matrix. This has proven reasonably accurate for coal.[23] Hence, the governing equation for gas flow, that accounts for both free- and adsorbed-gas phases can be defined as,

$$\left[\varphi_m + (1-\varphi_m)P_a\rho_c\frac{V_L P_L}{(p_m+P_L)^2}\right]\frac{\partial p_m}{\partial t} + \left(p_m - P_a\rho_c\frac{V_L p}{p+P_L}\right)\frac{\partial \varphi_m}{\partial t} - \nabla\left(D_g \nabla p_m\right) = 0 \quad [7]$$

where, $D_g$is the gas diffusion coefficient.

The diffusion coefficient may be obtained by fitting observations of pressure or gas mass with an appropriate analytical diffusivity model.[23] Moreover, the porosity, φ_m, is dependent on the adsorption-induced strain, thus the gas flow in the matrix is also coupled with the mechanical deformation.

3.1.3. Gas transfer between fracture and matrix

In the equidimensional DFM modelling, gas transmission between the sub-domains (i.e. Ω_f and Ω_m) accommodating transverse flow between fracture and the matrix are resolved as flux and pressure continuity across the fracture-matrix interface boundaries (i.e. Γ_{m,f_1} and Γ_{m,f_2}) *(see* Fig. 2 *(a))*[22];

$$q_{T,f}.\boldsymbol{n} = q_{T,m}.\mathrm{n} \qquad \text{on} \qquad \Gamma_{m,f_1} \text{ and } \Gamma_{m,f_2} \quad [8]$$

$$p_f = p_m \qquad \text{on} \qquad \Gamma_{m,f_1} \text{ and } \Gamma_{m,f_2} \quad [9]$$

where, $\boldsymbol{n}$ is the unit normal vector and $q_{T,i}$ is the transverse flow ($i = f, m$).

3.2. Mechanical system

3.2.1. Coal matrix deformation

The relationship linking infinitesimal strains to displacements for the elastic, homogeneous and isotopic coal matrix is defined as,

$$\varepsilon_{ij} = \frac{1}{2}\left(u_{i,j} + u_{j,i}\right) \quad [10]$$

where, ε_{ij} and u_i are the component of the total-strain tensor and the component of displacement, respectively.

Mechanical equilibrium is expressed as,

$$\sigma_{ij,j} + f_i = 0 \quad [11]$$

where, σ_{ij} and f_i are the component of the total-stress tensor and the component of body force, respectively.

The CO_2 interaction-induced mechanical deformation in the coal matrix is defined by a Navier-type equation for linear poro-elastic media, in which the adsorption-induced strain (ε_s) and the matrix pore pressure (p_m) are included as additional body forces. Since, ε_s is assumed to produce isotropic normal strains only, it is treated analogously to thermal expansion.[14] For a system that contains a single gas phase, the swelling strain, ε_s, can be expressed by a Langmuir-type model,[13,16,31] and is defined as;

$$\varepsilon_s = \varepsilon_L \frac{p_m}{p_m + P_L} \quad [12]$$

where, ε_L is the Langmuir volumetric strain constant.

Hence, the extended constitutive relation for the coal matrix deformation is given as,

$$\varepsilon_{ij} = \frac{1}{2G}\sigma_{ij} - \left(\frac{1}{6G} - \frac{1}{9K}\right)\sigma_{kk}\delta_{ij} + \frac{\alpha}{3K}p_m\delta_{ij} + \frac{\varepsilon_s}{3}\delta_{ij} \quad [13]$$

where α is the Biot's coefficient, $\sigma_{kk} = \sigma_{11} + \sigma_{22} + \sigma_{33}$ and δ_{ij} is the Kronecker delta, and G and K are the shear and bulk moduli of coal, defined as,

$$G = \frac{E}{2(1+\upsilon)} \quad [14]$$

$$K = \frac{E}{3(1-2\upsilon))} \quad [15]$$

where, E and υ are the Young's modulus and the Poisson's ratio of the coal matrix, respectively.

Combining Eqs. (10), (11) and (13) yields the Navier-type governing equation for coal matrix deformation,

$$Gu_{i,kk} + \frac{G}{1-2\upsilon}u_{k,ki} - \alpha p_{m,i} - K\varepsilon_{s,i} + f_i = 0 \quad [16]$$

that is coupled with the gas-transport system through matrix pore pressure.

3.2.2. Stresses on fracture-matrix interfaces and contact modelling with friction

The deforming fracture closes as a linear function of applied normal stress.[32] The fracture fluid pressure acts as a surface pressure on the fracture-matrix interface, modulating the fracture aperture through effective stress *(see* Fig. 2 *(b))*. Hence, both effects from fracture stiffness and fracture fluid pressure are applied as surface normal pressures on the fracture-matrix interfaces. It should be noted that the fracture stiffness can be best represented as a hyperbolic function with respect to fracture aperture. However, due to the large complexity of the geometric model and the fully-coupled process, a constant normal fracture stiffness is assumed in the current study. The relationship between the normal stress and the fracture closure can be expressed as,[20]

$$\sigma_n = \sigma_0 + \Delta p_f + K_n \Delta b \quad [17]$$

where, σ_n is the normal total stress, σ_0 is the initial total stress, $\Delta p_f (= p_f - P_0)$ is the change in gas pressure within the fracture, K_n is the normal fracture stiffness and $\Delta b (= b_0 - b)$ is the fracture closure. P_0 and b_0 are the initial pore pressure and the initial fracture aperture, respectively.

Contact pairs with frictional interfaces are defined at fracture-matrix interfaces, where the fracture surfaces are likely to contact due to full closure. The interface behaviour, where normal contact forces develop with fracture closure, is modelled with a no penetration rule using a penalty algorithm,[33] in order to avoid fracture inter-penetration. This method is more convenient, as the results are directly computed from the penalty stiffness and displacements, thus, no extra degrees of freedom are required to separately determine the contact pressure and the friction traction vector. The frictional interface is defined by a Coulomb friction model, in which the tangential stress required for sliding is expressed as,[34]

$$\tau = F\,\sigma_n^{'} \quad [18]$$

where, τ is the tangential stress, F is the coefficient of friction and $\sigma_n^{'}$ is the effective stress normal to the fracture surface.

The fully-coupled hydro-mechanical system described in this section is implemented in COMSOL Multiphysics software, validated and interpreted as a DFM geometric model, as explained in the following sections.

4. Model validation

The model is first validated against permeability results obtained from a lab-scale experimental study, conducted under *in-situ* stress conditions, on a single-fracture within coal, before extending the solution to a realistic fractured geometry *(see* Section 5*)*.

4.1. Model geometry and simulation procedure

The geometry for validation follows experimental details for flow along a longitudinally fractured core.[35] The CO_2 permeability experiment was conducted on a 38 mm in diameter × 76 mm in length cylindrical coal sample with an artificially induced-single fracture along its longitudinal axis. Fig. 3 (a) and (b) illustrate a plan view and a typical micro-CT cross-sectional image of the single-fractured coal sample, respectively. Accordingly, the DFM geometric model was defined with a single, longitudinal fracture with a constant fracture aperture of 1 mm, as shown in Fig. 3 (c). The required coal properties and the model parameters are obtained from the experimental study[35] and supplementary sources[36–39] as listed in Table 1. The fracture permeability was measured directly from the geometry and the fracture representing open pore space assumes a porosity of unity. In the experiment: 1) a confining pressure of 20 MPa was first applied to the sample to simulate in situ tri-axial stress conditions with, 2) a CO_2 injection pressure of 10 MPa then applied as a piecewise function to the base of the sample to simulate the gradual injection of CO_2 (from atmospheric pressure to 10 MPa, within 1 h). The model simulation was run until full pressure equilibration with the temporal evolution of average permeability calculated according to Eq. (4) and compared with the experimental results.

Table 1
Parameters used for validation.

Parameter	Value
Coal density (ρ_c) (kg/m^3)	1440
Matrix porosity (φ_m)	0.0075
Fracture porosity (φ_f)	1
Poisson's ratio (υ)	0.339
Young's modulus (E) (MPa)	3713
Normal fracture stiffness (K_n) (GPa/m)	60
Coefficient of friction (F)	0.6
Langmuir sorption constant (V_L) (m^3/kg)	0.0477
Langmuir pressure constant (P_L) (MPa)	8.44
Langmuir volumetric strain constant (ε_L)	0.029
Gas diffusion coefficient (D_g) (m^2/s)	3.76×10^{-10}
Biot's coefficient (α)	0.6
Temperature (T) (^oC)	25
Molar mass of CO_2 (M_g) (g/mol)	44.01
Density of CO_2 at STP (ρ_{CO_2}) (g/ml)	0.00196
Dynamic viscosity (μ) ($Pa.s$)	1.84×10^{-5}
Initial pore pressure (P_0) (MPa)	0.101325
Universal gas constant (R) ($J/mol.K$)	8.314

4.2. Modelling results

We compare experimental observations against calculations of the

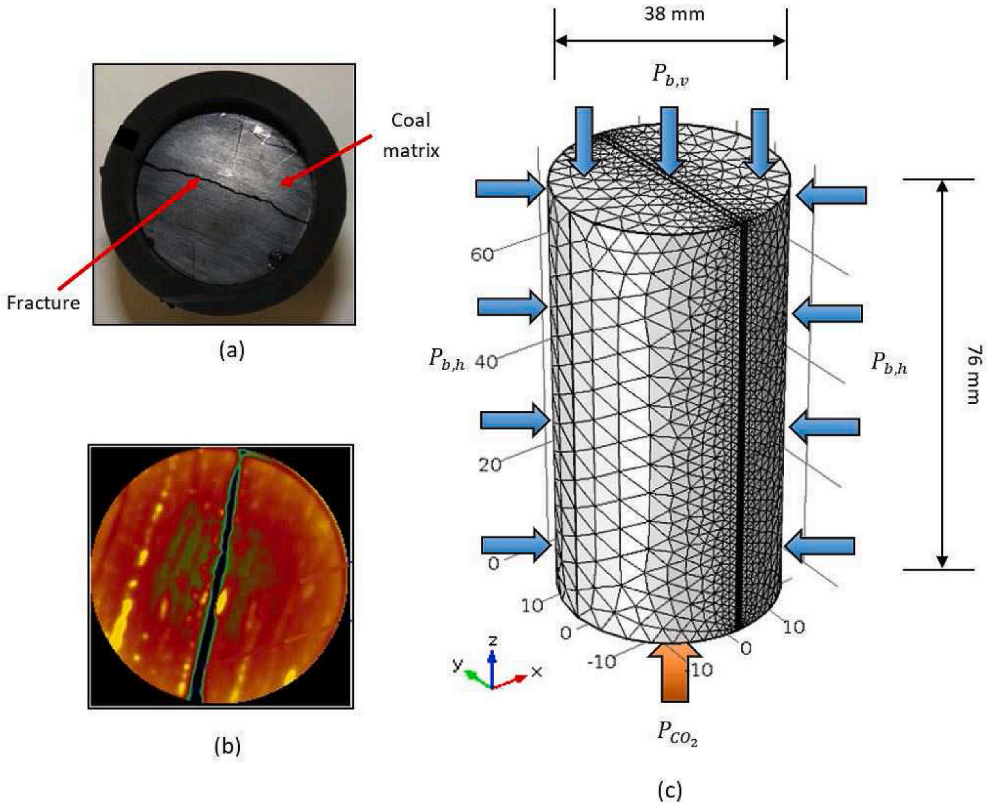

Fig. 3. a) Coal specimen in a rubber jacket containing a single longitudinal fracture, b) A typical CT scan of the fractured specimen, indicating fracture aperture (modified after Siriwardane et al.[35]) and c) The DFM geometric model utilized for the validation.

permeability ratio to validate the model. Fig. 4 illustrates the variation of permeability ratio with CO_2 interaction time. The direct comparison between simulation and experimental results indicate that the model is capable of successfully capturing the sense and magnitude of the permeability reduction and the variation of permeability ratio with CO_2 interaction time. It is apparent that a large permeability reduction occurs at the beginning of the injection and gradually reduces in rate of permeability reduction with increasing time. A 97.1% modelled reduction is observed after only ~27.5% of the total duration of the simulation, similar to the experimental observations. This is due to the immediate inception of matrix swelling with CO_2 injection,[40] rapidly closing fractures and consequently reducing the fracture permeability. Hence, the validation confirms the reliability of implementing the fully-coupled hydro-mechanical process in an equidimensional DFM model. We then extend this analysis to a complex fracture geometry.

4.3. Simulation of a complex DFM model

The validated simulation procedure is then applied to a complex DFM model, that represents a typical coal cleat network. Although the validation was completed on a model containing a single large fracture, the same modelling approach and the theoretical background are adopted in representing the complex DFM model - in order to confirm the reliability and the accuracy of the modelling results.

4.4. Model geometry and simulation procedure

A typical coal structure consists of an intricate orthogonal network of face and butt cleats. Face cleats are the most prominent cleat type that are persistent, widely-spread and laterally extensive. Conversely, butt cleats are formed after the extensive face cleats and terminate where they abut face cleats[3,41] (see Fig. 1 *(a)*). The complex spatial disposition of the cleat network induces a large heterogeneity within the coal seam, that requires the application of complex DFM modelling. Fig. 5 (a) shows a micro-CT image that illustrates the complex cleat system of a typical bituminous coal sample.[26] The cleat system itself is highly-disordered and complex, and thus difficult to represent in a 3D-DFM geometric model that incorporates the fully-coupled physical interactions, due to the excessive required computational burden. One possible way of circumventing this issue is to stochastically generate a simplified DFM model, while preserving the key attributes of the cleat structure, connectivity and aperture distribution.[42–44] Since many studies simply generate DFM models stochastically, only by considering statistical descriptions of the fracture network, they often disregard the original connectivity of face cleats and butt cleats. Such models are rendered incapable of accurately representing the actual coal cleat system. A novel method that overcomes this issue is by integrating fracture mechanics into a probabilistic framework.[26] This procedure mimics the natural cleat formation process to reproduce cleat network patterns (i.e. generating the face cleats first, followed by the butt cleats), thus is able to preserve the main structural and topological attributes of the cleat network. Fig. 5 (b) shows a stochastically reconstructed DFM model extracted from Jing et al.,[26] that was used in the current study to develop the 3D-DFM geometric model.

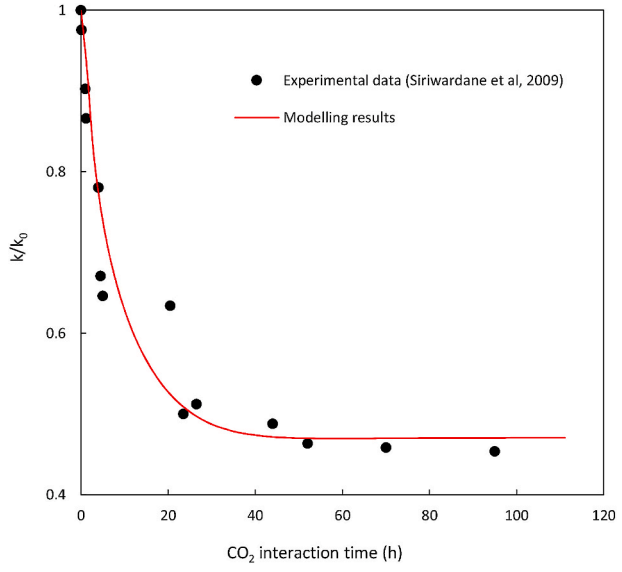

Fig. 4. Variation of permeability ratio with CO_2 interaction time: Modelling results fitted to experimental data from Siriwardane et al.[35]

The simplified fracture network shown in Fig. 5 (b) was used to generate an equidimensional DFM model by separating the fracture and matrix domains and defining the fracture-matrix interfaces while still preserving the local fracture aperture distribution and fracture connectivity. To define more realistic boundary conditions, the coal mass was modelled in three-dimensions by extruding the 2D geometry. The fractures were generated as smooth and straight fractures and the sharp edges at interconnections were minimized to the fullest extent to reduce the geometric and meshing complexity, and subsequently the computational intricacy and burden. The generated 3D-geometry was then re-scaled to represent a lab-scale coal specimen with the final dimensions of 76 mm × 82 mm × 5 mm and with fracture aperture ranging from 0.2 mm to 1 mm *(see* Fig. 5 *(c))*. The meshed geometry is the next important step that controls the fidelity of the model in representing the fracture geometry, solution accuracy and computational burden. Fig. 6 (a) shows the meshed-model, in which a finer mesh is adopted toward matrix-fracture interfaces (i.e. fractures) to improve the accuracy and a combination of element types were used to generate the complete mesh. The mesh comprises 20717 tetrahedral elements, 11897 triangular elements, 2610 edge elements and 406 vertex elements, with the maximum element size limited to 7.2 mm.

A gas diffusion coefficient (D_g) of 6.58 × 10^{-11} m^2/s, temperature (T) of 40 °C, matrix porosity (φ_m) of 0.0237, Langmuir volumetric strain constant (ε_L) of 0.0256 and normal fracture stiffness (K_n) of 5 GPa/m were used in the simulation with other mechanical and hydraulic properties similar to those given in Table 1. Boundary displacement conditions were applied to the model including constrained displacements in all directions at the base and constrained displacements in the x- and y-directions at the side walls to mimic *in-situ* reservoir conditions.[20,33] For the boundary stress conditions, an overburden stress ($P_{b,v}$) of 15 MPa was applied at the top surface and a horizontal stress ($P_{b,h}$) of 12 MPa was assigned to the side walls to replicate an extensional tectonic regime[33] *(see* Fig. 6 *(a))*. A CO_2 injection pressure was applied to one side of the model as a piecewise incremented function. The simulation was run until full pressure equilibrium with temporal and spatial analyses completed by considering five points of interest, distributed throughout the geometry as shown in Fig. 6 (b).

4.5. Modelling results

The temporal and spatial analyses are conducted in terms of the evolution of fracture and matrix pressures, adsorbed mass of CO_2, matrix volumetric swelling, fracture aperture and permeability, and contact pressures within the model. Moreover, the results are compared with the case of absent swelling (no-swelling behaviour), in order to emphasize the significance of CO_2-induced coal matrix swelling on the overall flow behaviour.

4.5.1. Pore pressure evolution

Fig. 7 shows the evolution of the pressure distribution throughout the coal mass at different times. This clearly exhibits the rapid flow of CO_2 through the fracture network, due to its high permeability, compared to the slow diffusion into the coal matrix. The injected CO_2

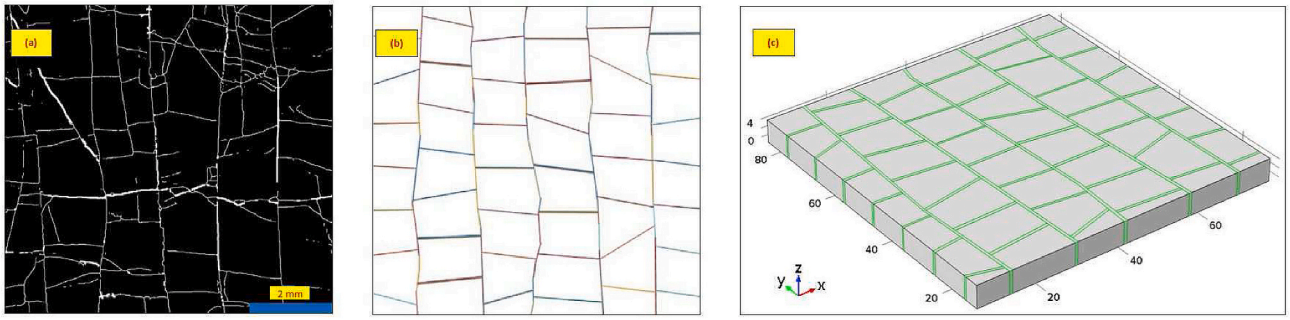

Fig. 5. a) Original micro-CT image, illustrating the complex fracture network, b) Stochastically simplified and reconstructed DFM model (extracted from Jing et al.[26]), and c) Extruded and re-scaled 3D-geometric model used for the simulation.

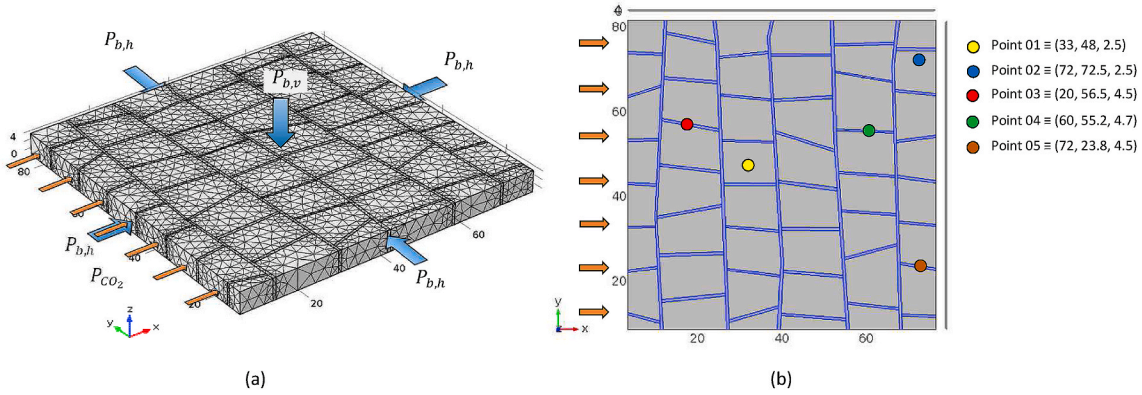

Fig. 6. a) Geometric model, indicating the meshing, boundary pressures and the location of CO_2 injection, and b) Plan view of the geometry, indicating the points of interest used to analyse spatial variations in simulation variables.

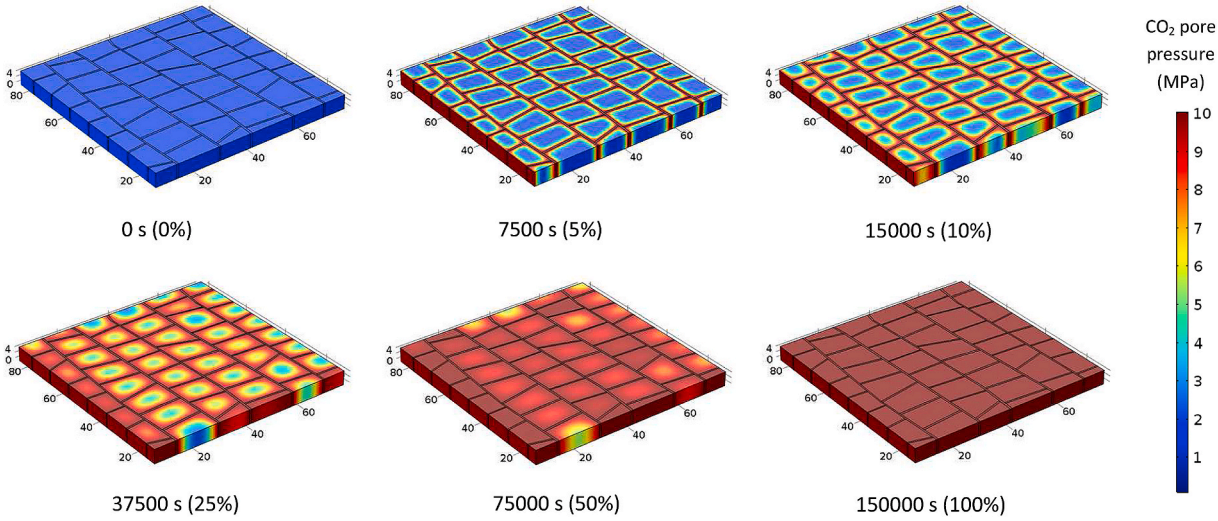

Fig. 7. Temporal and spatial variation of CO_2 pore pressure development in the coal mass.

first flows through the high-permeability fractures then diffuses into the coal matrix from the fracture-matrix interfaces. The colour bar displays the CO_2 pore pressure values, ranging from atmospheric pressure at the beginning of the simulation to 10 MPa at full pressure equilibrium. Since the geometry represents a lab-scale sample, it takes only a minute time to fully penetrate the major interconnected fractures in the network to equilibrium pressure. This is clearly shown in Fig. 8 (a), illustrating the evolution of fracture pressure with time at three points of interest in the fracture domain. It is notable that all three points follow a similar trend in pressure development without exhibiting any difference over this specific time scale, irrespective of their spatial disposition in the fracture domain. This is because the fractures are open (porosity of unity) and the fracture permeability is calculated from the parallel-plate law *(see* Eq. (4)*)*, which in turn yields a high fracture permeability. This would be different if the initial fracture permeability is low, possibly due to the presence of granular infill. In that case, the fracture permeability would be better defined in terms of an effective diameter of the filling grains representing the pore throat diameter,[45] which may then defined as a

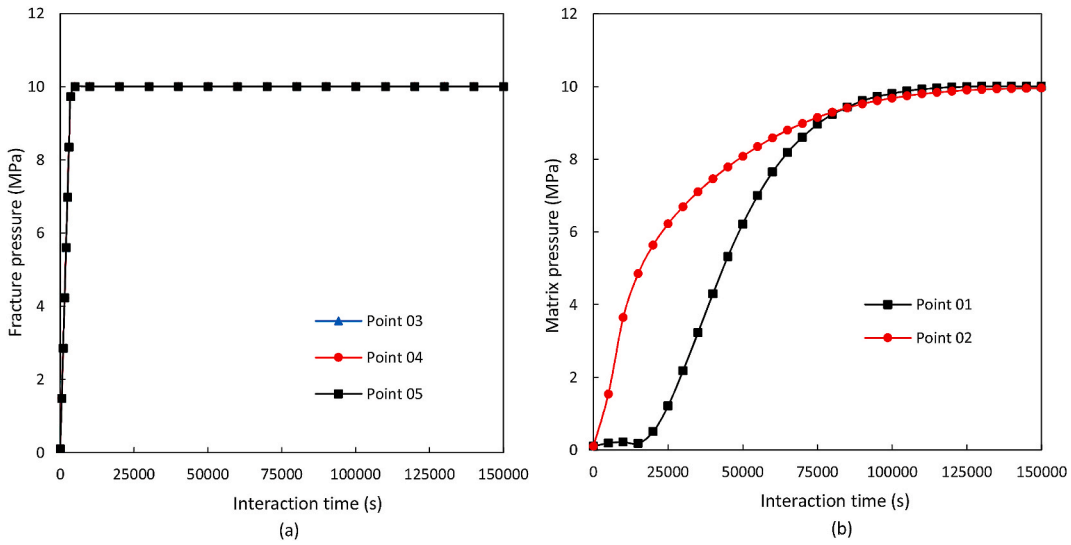

Fig. 8. Variation of a) Fracture pressure and b) Matrix pressure with CO_2 interaction time.

function of the initial fracture permeability and change in the local fracture aperture.[46,47]

In contrast, since the matrix domain exhibits a delayed-pore pressure development due to its low diffusivity, it is possible to clearly differentiate the spatial signatures of pressure evolution in the matrix domain, within the defined time frame. For instance, as shown in Fig. 8 (b), the pressure development at point 02 is more rapid at the beginning than point 01. This is because, although point 02 is further away from the CO_2 injection point, it is closer to an interface with a high-permeability fracture – that provides a rapid pathway for the CO_2 to reach that point. Conversely, point 01 is located in the centre of a coal matrix block, that hinders rapid access for the CO_2, delaying pressure development *(see Fig. 6 (b))*. However, this temporal variation also depends on the diffusive properties (i.e. gas diffusion coefficient (D_g)) of the coal matrix – thus should be precisely determined through an experimental analysis. Overall, this spatial analysis emphasizes the importance of the existing fracture network on the complex pore pressure development within the coal mass, that can only be resolved through a DFM modelling approach.

4.5.2. *Adsorbed mass of CO_2 and evolution of matrix swelling*

Measurements defining the adsorbed mass of CO_2 and matrix swelling are vital in the context of CO_2 geo-sequestration, as they control the amount of CO_2 that can be effectively stored in a certain coal reservoir – this then governs the efficiency and the long-term feasibility of the project. The total adsorbed mass depends on the adsorption potential and the available adsorption sites within the coal matrix blocks. The adsorptive mass is controlled by the sorption response with rates controlled by diffusion coefficient and block size – larger diffusion coefficients and smaller block sizes/fracture spacing promote more rapid sorption. Since the complex DFM model consists of several coal matrix

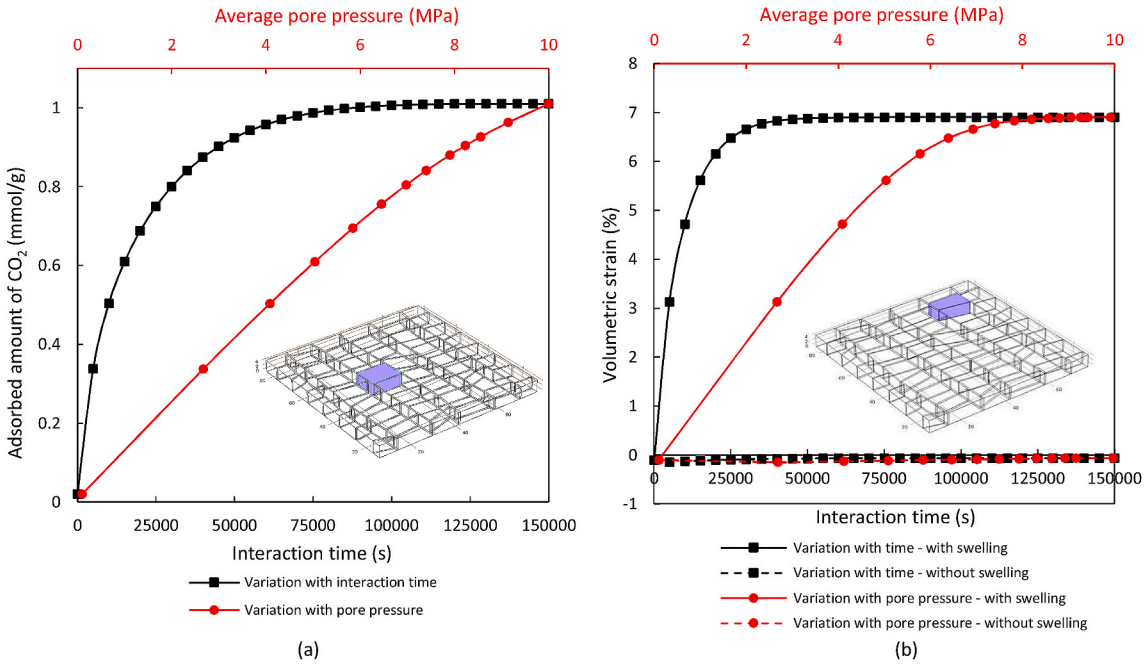

Fig. 9. a) Variation of the adsorbed mass of CO_2 in a selected coal matrix block with CO_2 interaction time and with average CO_2 pore pressure and, b) Variation of the volumetric strain of a selected coal matrix block with CO_2 interaction time and with average CO_2 pore pressure. Note that the strain results are plotted together for cases both with- and without-swelling, for direct comparison.

blocks with different shapes and sizes, we selected single matrix blocks to comprehensively analyse the adsorbed amount and the volumetric swelling *(highlighted in Fig. 9)*. The adsorbed amount of CO_2 in a particular coal matrix block at time t ($m_{a(t)}$) is quantified through the volume integration of the selected matrix block, as.[23,48]

$$m_{a(t)} = \iiint \left| (1-\varphi_m)\frac{M_g P_a}{RT}\rho_c \frac{V_L p_m}{p_m + P_L}\right|_t \quad [19]$$

Fig. 9 (a) illustrates the variation of the adsorbed amount of CO_2 in the selected matrix block with CO_2 interaction time and with the average pore pressure. It is apparent that the adsorbed mass initially increases rapidly but gradually asymptotes to a constant with increasing interaction time, as the matrix block reaches pressure equilibrium. Moreover, the adsorbed mass shows a near-linear increment with the average pore pressure. This is since sorption is linearly related to pressure in the early stages of Langmuir sorption. This deviates from the linear trend near pressure equilibrium at higher relative pressures as all the available adsorption sites are occupied.

Fig. 9 (b) shows the variation in volumetric strain of the selected coal matrix block with CO_2 interaction time and for an average pore pressure, in which the results are compared with the no-swelling behaviour – that represents the response to a non-sorbing gas (e.g. He or N_2). The initial volumetric strain of the matrix block is slightly negative, implying shrinkage, due to the compression driven by the applied fracture fluid pressure on the fracture-matrix interfaces. The rapid fluid pressure permeation through the high-permeability fracture domain creates an additional surface pressure on all matrix boundaries, causing universal shrinkage at the beginning of injection. However, this is gradually overcome by the diffusion and adsorption-induced swelling of the coal matrix, resulting in an overall volume expansion at the full pressure equilibrium. The final sorption-induced swelling is significantly larger than the initial surface pressure-induced shrinkage *(see Fig. 9 (b))*. In the absence of swelling behaviour, the volumetric strain begins negative with the initial injection then rebounds to near null as the pressure equilibrates. This is a consequence of initial compaction of the block as the fracture pressure applies a large effective stress on the block, that ultimately dissipates as fluid permeates the block and the effective stresses between block and fracture equilibrate. The differences in strains for sorbing and non-sorbing gases clearly distinguishes the impacts of a highly-reactive gas (i.e. CO_2) with that of a relatively non-reactive gas like N_2. Further, it is apparent that the volumetric strain caused by the adsorption is significantly faster than the accumulation of matrix pressure shown in Fig. 8 (b). This may be related to the rapid adsorption of CO_2 and the consequent swelling that occurs during coal-CO_2 interaction. In fact, CO_2 adsorbs rapidly on to the coal matrix during CO_2 injection,[40] causing immediate coal matrix swelling, as soon as the interaction takes place. This in turn may possibly induce large swelling strains in coal even at relatively low pore pressures.

The sorption-induced volumetric swelling or the volume expansion of individual matrix blocks can significantly affect the local fracture aperture and subsequently the flow behaviour, which is further discussed in the following section. In our theoretical approach, the adsorbed mass of CO_2 and the matrix swelling are modulated by Langmuir-type equations, where the two phenomena are dependent on the Langmuir sorption constant (V_L) and the Langmuir volumetric strain constant (ε_L), respectively. Hence, the values of the two parameters should be precisely determined experimentally for any given coal rank, before incorporating them in the fully-coupled hydro-mechanical model, as the coupled process is controlled by the two parameters.

4.5.3. Evolution of fracture aperture and fracture permeability variation

Fracture permeability, defined as a function of fracture aperture is an important parameter that governs gas flow behaviour in fractured reservoirs. The fracture aperture in the coal reservoir is stress-dependent and varies with a change in both the effective stress and the magnitude of sorption-induced swelling. A major advantage of DFM modelling is that the spatial and localized changes in fracture aperture can be efficiently evaluated, as the fracture network is defined explicitly in the geometric model.

Fig. 10 shows the fracture network comprising both face and butt cleats, representative of the cleat system of a typical coal reservoir. The local fracture aperture is measured directly from the geometry, as the distance between the bounding matrix walls. The fracture network consists of fractures with the apertures ranging from 0.2 mm to 1 mm, whereas the apertures of the face cleats are greater than 0.5 mm in the original geometry (see Fig. 10 (a)). A direct comparison between the original and the fully-CO_2-interacted fracture network implies that apertures of both face and butt cleats have been reduced significantly following CO_2 exposure, due to the adsorption-induced swelling of the adjacent matrix blocks. In fact, some fractures are near-completely closed due to their initial very low fracture aperture and the swelling behaviour of the bounding matrix (see Fig. 10 (b)). It should be noted that, since the displacements of the basal boundaries are constrained at all directions, fracture apertures at this basal plane remain constant throughout the injection. Fig. 11 shows the temporal variation of local fracture aperture at three points of interest in the fracture domain (see Fig. 6 (b)), including one near fully-closed fracture (i.e. point 04). Again, the fractures dilate slightly as the injection pressure is applied and immediately/rapidly permeates the fracture network. This is congruent with the volumetric swelling results, in which the matrix blocks show a slight shrinkage at the beginning, causing this slight increase in aperture (see Fig. 9 (b)). Importantly, since we adopt a no-penetration rule for the contact modelling, the separation between fracture walls remains zero at full-closure, without being negative, since no inter-penetration between the two bounding matrix walls is allowed during the swelling deformation. This is an accurate representation of real response. Furthermore, the dotted-lines of Fig. 11 indicate the fracture aperture variation in absent-swelling, where the final deformations are small, by comparison with the case for swelling.

In single- or multi-continuum modelling and analytical approaches, the variations of fracture aperture or permeability with the pore pressure increment are often analysed without accommodating details of the spatial geometry and heterogeneity. However, in a fractured reservoir, the local fracture aperture and permeability are critically dependent on the deformation of the coal matrix in the vicinity of the fracture, rather than on the overall reservoir behaviour. This factor is explicitly accommodated in DFM approaches where variation in the aperture of three fractures of interest are plotted against the average pore pressure developed in the bounding coal matrix (see Fig. 12). It is apparent that the fracture aperture reduces significantly with increasing average pore pressure in the bounding coal matrix, due to matrix swelling. Crucially, the magnitude of local aperture reduction depends on the shape, size and the swelling potential of bounding matrix block, thus they vary from fracture to fracture. For instance, the fracture apertures are reduced by 66%, 99% and 75% at points 3, 4 and 5, respectively. This clearly demonstrates that the hydro-mechanical behaviour of fractured reservoirs is highly-localized, and that accurate representation of this behaviour relies upon explicit descriptions of fracture geometry.

Fig. 13 shows the temporal variation of fracture permeability ratio at three points of interest in the fracture domain, both with- and without-swelling behaviour. Since fracture permeability is defined as a function of local fracture aperture, the evolution of permeability follows a similar trend to that for aperture variation. Permeability reduces significantly with CO_2 interaction, due to adsorption-induced swelling. This is consistent with prior results obtained by Bertrand et al.,[20] in which they have used the multi-dimensional DFM modelling approach to analyse the permeability variation of CO_2-interacted fractured coal. In fact, they have observed a similar trend in permeability reduction with CO_2 interaction time, which is caused by the change in effective stress and the adsorption-induced swelling. The early-time permeability change is detailed in the zoomed-in inset of Fig. 13, which highlights the slight

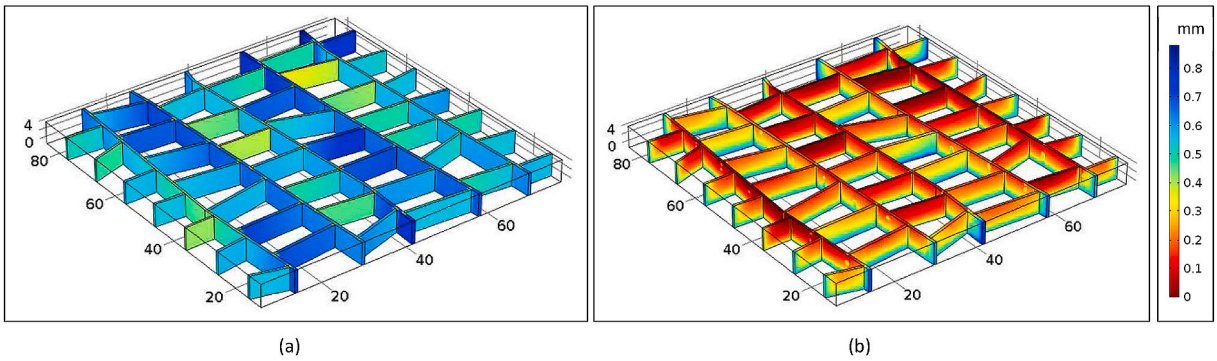

Fig. 10. Spatial variation of fracture aperture: a) Before CO_2 injection (at 0 s) and, b) After full pressure equilibration (at 150000 s).

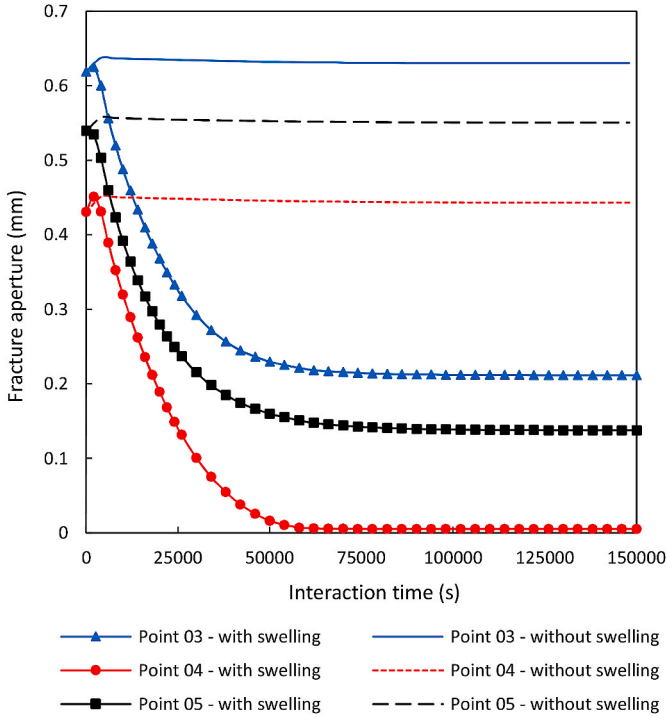

Fig. 11. Temporal variation of fracture aperture both with- and without-swelling.

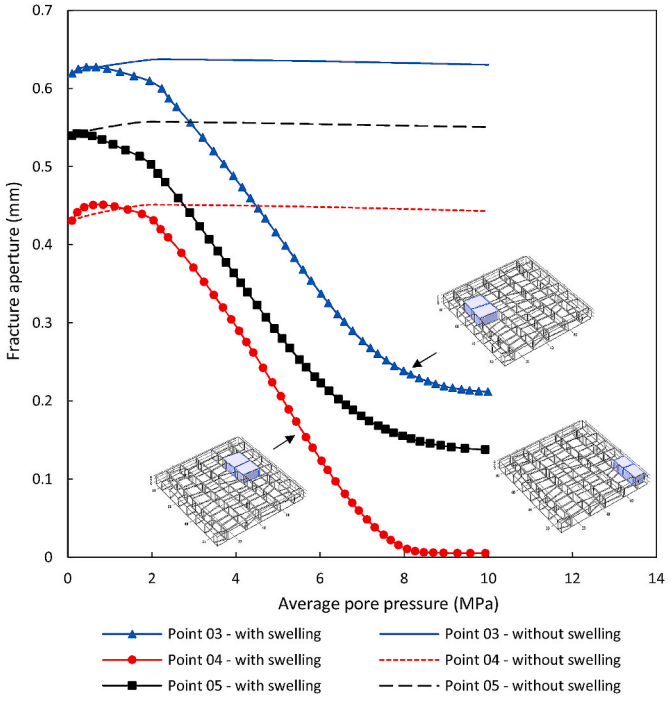

Fig. 12. Variation of fracture aperture with average pore pressure in the bounding coal matrix.

permeability increase due to the initial injection – caused by the fluid pressure applied on the bounding walls of the fracture and compression of the matrix. The permeability of some fractures (i.e. at point 04) reduces to almost zero, due to near full-closure of the respective fracture. Such changes in permeability of the fracture network will result in large changes in both permeability and especially in permeability anisotropy. These changes will significantly impact flow behaviour in the coal seam to further CO_2 injection phases, ultimately hindering CO_2 injectivity and therefore the feasibility of the sequestration projects.

4.5.4. Evolution of fracture contact pressures

Depending on the initial fracture aperture and the swelling deformation of the bounding matrix, some fractures may fully close at maximum pressures – resulting in significant contact pressures. The fracture walls are defined as frictional interfaces and the contact pairs retained separated by a no-penetration *(see* Sections 3.2.2 and 5.2.3*)*. The magnitude of the contact pressure depends competitively on the boundary pressure, fracture fluid pressure and swelling-induced stress. Fig. 14 illustrates the locations and the magnitudes of the resulting contact pressures, that directly indicates the locations of the near fully-closed fractures in the complex geometry. Noticeably, the butt cleats preferentially close to zero apertures over the face cleats. The lack of closure of fractures at the base of the model domain is merely an artefact of the full displacement restraint boundary condition applied on that boundary. Fig. 15 shows the temporal variation of the maximum normal contact pressure on a selected fracture. Initially, the contact pressure remains small (zero) until the two surfaces contact, and then increases continuously with further swelling of the bounding matrix, until the system reaches pressure and swelling equilibria within the matrix. The point of initiation and the magnitude of the evolving contact pressures varies spatially, depending on the local hydro-mechanical properties of the fractures and matrix. Further, one should pay special attention when selecting the boundary conditions, including displacement and stress conditions, as they can largely affect the overall mechanical deformation of the model and therefore the entire CO_2 flow behaviour. The most appropriate and realistic boundary conditions should be defined to accurately model the entire process.

Overall, the current DFM model of a representative coal mass with a complex fracture network suggests that CO_2 interaction-induced hydro-mechanical response is highly sensitive to fracture geometry and connectivity – in addition to the manifestation of complex physical-

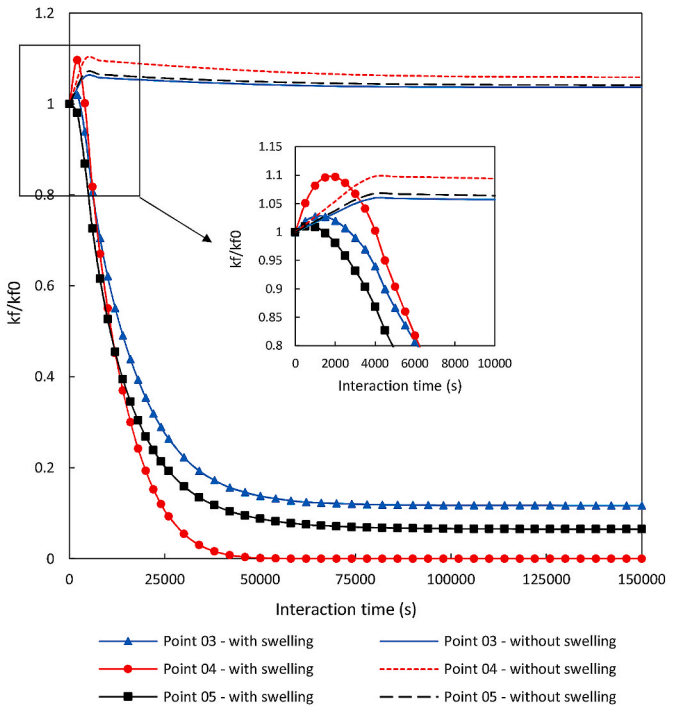

Fig. 13. Temporal variation of fracture permeability ratio both with- and without-swelling.

couplings and feedbacks. The use of an equidimensional DFM modelling approach accommodates realistic fully-coupled processes by further including the development of contact forces and frictional forces on the fracture walls as the fractures fully close. Furthermore, since fracture permeability is defined as a function of local fracture aperture, where the aperture is measured from the deformed geometry at each solution step, it provides an accurate path to the time-dependent solution. The use of micro-CT images to constrain the key attributes of real fracture networks in coal, including fracture apertures, interconnectivity, and the structure of face and butt cleats provides a more accurate approach to model the realistic flow behaviour in fractured coal. Note that the computational burden for direct equidimensional DFM modelling of the micro-structure at reservoir scale would be prohibitive. However, the stochastically-developed lab-scale geometric model presented in the current study is useful in understanding key characteristics and controls of a representative elementary volume and presents a strong foundation for explicit DFM modelling of the hydro-mechanical behaviour of CO_2-interactions in coal.

5. Conclusions

An equidimensional DFM modelling approach is adopted to model the fully-coupled CO_2 flow – deformation process in a representative elementary volume of a fractured coal mass. The evolution of fracture/matrix pressures, adsorbed mass of CO_2, adsorption-induced volumetric swelling, change in local fracture aperture and permeability and development of contact stresses are specifically analysed through an explicit geometric model. The following conclusions are made, based on the simulation results:

The geometry and connectivity of the natural cleat system exerts a first-order control on CO_2 flow behaviour in coal, in which CO_2 flow

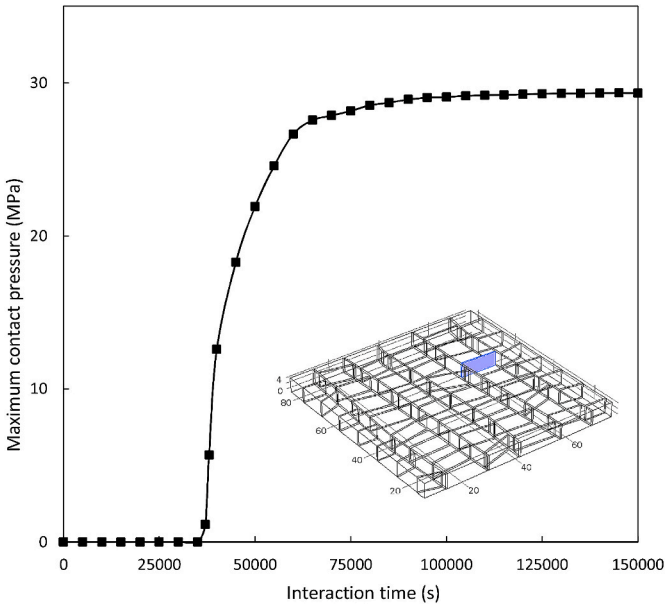

Fig. 15. Variation of maximum contact pressure with CO_2 interaction time within a fully-closed fracture.

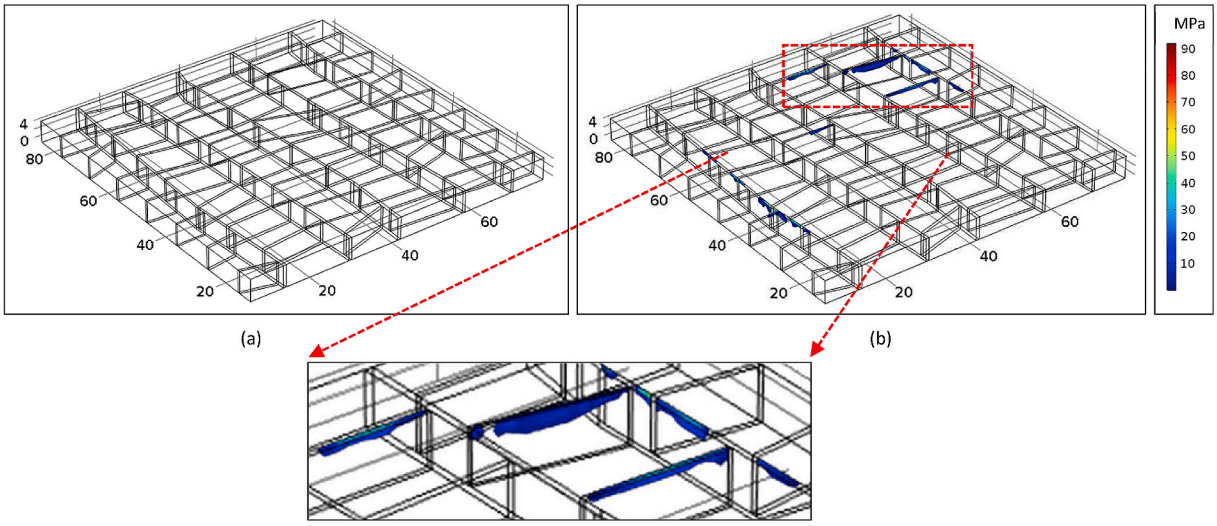

Fig. 14. Spatial variation of normal contact pressure: a) Before CO_2 injection (at 0 s) and, b) After full pressure equilibration (at 150000 s), indicating the locations of fully-closed fractures.

through a connected fracture network provides rapid pathways for CO_2 migration through the reservoir and thereby to coal matrix blocks. The distribution of fracture network affects the temporal and spatial rates of saturation of the corresponding coal matrix blocks. The highly-permeable fracture network percolates near immediately, compared to the low rate of diffusive transport into the matrix blocks. Hence, pressure development in the near-fracture regions of the matrix material is relatively rapid, compared to their interior. Individual matrix blocks exhibit a slight shrinkage in early-time due to the fracture fluid pressure applied to the matrix boundaries. This initial shrinkage is countered as adsorption-induced volumetric swelling dominates in later-time, resulting in a net volume expansion at full pressure equilibration. The fully-coupled simulation affirms that CO_2 adsorption-induced swelling of the coal matrix dominates the response and reduced rates of CO_2 injection into the interior of the reservoir. This results as the volume expansion of the matrix blocks reduces the local fracture aperture and therefore the fracture permeability. As introduced in this study, the real-time evaluation of fracture aperture and consequent fracture permeability is important when simulating the fully-coupled time-dependent process. Furthermore, depending on the initial fracture aperture and the swelling behaviour of the bounding matrix, some fractures may near-fully close, drastically reducing local permeability and significantly increasing permeability anisotropy. These factors will significantly impact CO_2 injectivity. Specifically, this equidimensional DFM modelling approach, incorporating robust accommodation of fracture contact mechanics identifies the locations of full fracture closure during CO_2 injection – these closing fractures are preferentially butt cleats - due to their originally smaller fracture apertures. Overall, the results suggest that the CO_2 interaction-induced flow modifications in a fractured coal reservoir is a highly-complex and localized process and is thus best resolved through fully-coupled DFM modelling.

Declaration of competing interest

The authors declare that they have no known competing financial interests or personal relationships that could have appeared to influence the work reported in this paper.

References

1 Bp, Statistical. *Review of World Energy*. *68th edition* 2019.
2 Enerdata. *Energy-related CO_2 Emissions 2019 Estimates - Analyst Brief*. Enerdata Executive Brief; 2019.
3 Sampath KHSM, Perera MSA, Ran, , et alTao X. *CH_4-CO_2 gas exchange and supercritical CO_2 based hydraulic fracturing as CBM production-accelerating techniques: a review*. *J CO_2 Util*. 2017;22:212–230.
4 Pan Z, Connell LD. A theoretical model for gas adsorption-induced coal swelling. *Int J Coal Geol*. 2007;69(4):243–252.
5 Durucan S, Shi JQ. *Improving the CO_2 well injectivity and enhanced coalbed methane production performance in coal seams*. *J Coal Geol*. 2009;77(1):214–221.
6 Harpalani S, Chen G. Influence of gas production induced volumetric strain on permeability of coal. *Geotech Geol Eng*. 1997;15(4):303–325.
7 Gray I. Reservoir engineering in coal seams: Part 1-The physical process of gas storage and movement in coal seams. *SPE Reservoir Eng*. 1987;2(1):28–34.
8 Perera M, Ranjith P, Airey D, Choi S-K. Sub-and super-critical carbon dioxide flow behavior in naturally fractured black coal: an experimental study. *Fuel*. 2011;90(11):3390–3397.
9 Oudinot AY, Koperna GJ, Philip ZG, Liu N, Heath JE, Wells A, Young GB, Wilson T. *CO_2 injection performance in the Fruitland coal fairway, San Juan Basin: results of a field pilot*. *SPE J*. 2011;16:864–879, 04.
10 Ranathunga AS, Perera MSA, Ranjith PG, Jub Y, Vishal V, Silva PNKD. *A macro-scale experimental study of sub- and super-critical CO_2 flow behaviour in Victorian brown coal*. *Fuel*. 2015;158:864–873.
11 Wu Y, Liu J, Elsworth D, Siriwardane H, Miao X. Evolution of coal permeability: contribution of heterogeneous swelling processes. *Int J Coal Geol*. 2011;88(2-3):152–162.
12 Pekot LJ, Reeves SR. *Modeling coal matrix shrinkage and differential swelling with CO_2 injection for enhanced coalbed methane recovery and carbon sequestration applications*. In: *Topical Report*. U.S. Department of Energy; 2002.
13 Robertson EP, Christiansen RL. *A Permeability Model for Coal and Other Fractured, Sorptive-Elastic Media*. Idaho National Laboratory (INL); 2006.
14 Palmer I, Mansoori J. How permeability depends on stress and pore pressure in coalbeds: a new model. In: *SPE Annual Technical Conference and Exhibition*. Society of Petroleum Engineers; 1996.
15 Seidle J, Jeansonne M, Erickson D. Application of matchstick geometry to stress dependent permeability in coals. In: *SPE Rocky Mountain Regional Meeting*. Society of Petroleum Engineers; 1992.
16 Cui X, Bustin RM. Volumetric strain associated with methane desorption and its impact on coalbed gas production from deep coal seams. *AAPG Bull*. 2005;89(9):1181–1202.
17 Shi J, Durucan S. Drawdown induced changes in permeability of coalbeds: a new interpretation of the reservoir response to primary recovery. *Trans Porous Med*. 2004;56(1):1–16.
18 Hyman JD, Karra S, Makedonska N, Gable CW, Painter SL, Viswanathan HS. dfnWorks: a discrete fracture network framework for modeling subsurface flow and transport. *Comp Geo*. 2015;84:10–19.
19 Wang H. Discrete fracture networks modeling of shale gas production and revisit rate transient analysis in heterogeneous fractured reservoirs. *J Petrol Sci Eng*. 2018;169:796–812.
20 Bertrand F, Buzzi O, Collin F. Cleat-scale modelling of the coal permeability evolution due to sorption-induced strain. *Int J Coal Geol*. 2019;216:103320.
21 Berre I, Doster F, Keilegavlen E. Flow in fractured porous media: a review of conceptual models and discretization approaches. *Trans Por Med*. 2019;130(1):215–236.
22 Tunc X, Faille I, Gallouët T, Cacas MC, Havé P. A model for conductive faults with non-matching grids. *Comp Geo*. 2012;16(2):277–296.
23 Sampath KHSM, Perera M, Matthai S, Ranjith P, Dong-yin L. *Modelling of fully-coupled CO_2 diffusion and adsorption-induced coal matrix swelling*. *Fuel*. 2020;262:116486.
24 Shi J, Durucan S. *CO_2 storage in deep unminable coal seams*. *Oil Gas Sci Technol*. 2005;60(3):547–558.
25 Ma Q, Harpalani S, Liu S. A simplified permeability model for coalbed methane reservoirs based on matchstick strain and constant volume theory. *Int J Coal Geol*. 2011;85(1):43–48.
26 Jing Y, Armstrong RT, Ramandi HL, Mostaghimi P. Coal cleat reconstruction using micro-computed tomography imaging. *Fuel*. 2016;181:286–299.
27 Darcy H.P.G., Les Fontaines publiques de la ville de Dijon. Exposition et application des principes à suivre et des formules à employer dans les questions de distribution d'eau, *etc*. 1856: V. Dalamont.
28 Witherspoon PA, Wang JS, Iwai K, Gale JE. Validity of cubic law for fluid flow in a deformable rock fracture. *Wat Reso Res*. 1980;16(6):1016–1024.
29 Crank J. *The Mathematics of Diffusion*. Oxford university press; 1979.
30 Saghafi A, Faiz M, Roberts D. *CO_2 storage and gas diffusivity properties of coals from Sydney Basin, Australia*. *Int J Coal Geol*. 2007;70(1-3):240–254.
31 Harpalani S, Schraufnagel RA. Shrinkage of coal matrix with release of gas and its impact on permeability of coal. *Fuel*. 1990;69(5):551–556.
32 Lepillier B, Daniilidis A, Gholizadeh ND, Bruna P-O, Kummerow J, Bruhn D. A fracture flow permeability and stress dependency simulation applied to multi-reservoirs, multi-production scenarios analysis. *Geoth Energy*. 2019;7(1):24.
33 Agheshlui H, Sedaghat MH, Matthai S. Stress influence on fracture aperture and permeability of fragmented rocks. *J Geophys Res: Sol Ear*. 2018;123(5):3578–3592.
34 Coulomb CA. Sur une application des regles de maximums et minimums a quelques problemes de statistique relatifs a larchitesture. *Académie Royale de Science Memorie Mechanics and Mining Sciences*. 1773;7:343–382.
35 Siriwardane H, Haljasmaa I, McLendon R, Irdi G, Soong Y, Bromhal G. Influence of carbon dioxide on coal permeability determined by pressure transient methods. *Int J Coal Geol*. 2009;77(1-2):109–118.
36 Robertson EP, Christiansen RL. *Modeling Permeability in Coal Using Sorption-Induced Strain Data*. Idaho National Laboratory (INL); 2005.
37 Mazumder S, Wolf K, Van Hemert P, Busch A. Laboratory experiments on environmental friendly means to improve coalbed methane production by carbon dioxide/flue gas injection. *Trans Por Med*. 2008;75(1):63–92.
38 Masoudian MS, Airey DW, El-Zein A. *Experimental investigations on the effect of CO_2 on mechanics of coal*. *Int J Coal Geol*. 2014;128:12–23.
39 Kang J, Zhang B, , et alKang T. Mechanical testing of anthracite to assess its surface energy and temperature dependence. *Fuel*. 2019;239:76–86.
40 Karacan CÖ. *Heterogeneous Sorption and Swelling in a Confined and stressed Coal during CO_2 injection*. *Energy Fuels*. 2003;17(6):1595–1608.
41 McCulloch CM, Deul M, Jeran PW. *Cleats in Bituminous Coalbeds*. Pittsburgh, Pa.: U.S. Bureau of Mines: Pittsburgh Mining and Safety Research Center; 1974.
42 Elmo D, Rogers S, Stead D, Eberhardt E. Discrete Fracture Network approach to characterise rock mass fragmentation and implications for geomechanical upscaling. *Mineral Tech*. 2014;123(3):149–161.
43 Gao F, Stead D, Kang H. Numerical investigation of the scale effect and anisotropy in the strength and deformability of coal. *Int J Coal Geol*. 2014;136:25–37.
44 Cacas M-C, Ledoux E, de M, decerf P. Modeling fracture flow with a stochastic discrete fracture network: calibration and validation: 1. The flow model. *Water Resour Res*. 1990;26(3):479–489.
45 Zhang S, Liu J, Wei M, Elsworth D. Coal permeability maps under the influence of multiple coupled processes. *Int J Coal Geol*. 2018;187:71–82.
46 Liu J, Elsworth D, Brady B. Linking stress-dependent effective porosity and hydraulic conductivity fields to RMR. *Int J Rock Mech Min Sci*. 1999;36(5):581–596.
47 Chilingar GV. Relationship between porosity, permeability, and grain-size distribution of sands and sandstones. In: *Developments in Sedimentology*. Elsevier; 1964:71–75.
48 Wang G, Ren T, Qi Q, Lin J, Liu Q, Zhang J. Determining the diffusion coefficient of gas diffusion in coal: development of numerical solution. *Fuel*. 2017;196:47–58.